Chinese Chemical Letters 33 (2022) 3539–3542

Contents lists available at ScienceDirect

Chinese Chemical Letters

journal homepage: www.elsevier.com/locate/cclet

Hierarchical assembly of uranyl metallacycles involving macrocyclic hosts

Yuanyuan Liang[a,b], Lei Mei[a,*], Qiuyan Jin[a,b], Junshan Geng[a], Jingyang Wang[a], Kang Liu[a], Kongqiu Hu[a], Jipan Yu[a], Weiqun Shi[a,*]

[a] Laboratory of Nuclear Energy Chemistry, Institute of High Energy Physics, Chinese Academy of Sciences, Beijing 100049, China
[b] University of Chinese Academy of Sciences, Beijing 100049, China

ARTICLE INFO

Article history:
Received 31 January 2022
Revised 20 March 2022
Accepted 21 March 2022
Available online 24 March 2022

Keywords:
Metallacycle
Coordination self-assembly
Uranyl
Cucurbituril
Hierarchical structure
Molecular necklace

ABSTRACT

Actinide metallacycles are an emerging class of functional coordination assemblies, but multi-level assembly from metallacycle units toward hierarchical supramolecular structures are still rarely investigated. In this work, we put forward a novel supramolecular inclusion-based method through introducing two macrocyclic hosts, cucurbit[7]uril (CB[7]) and cucurbit[8]uril (CB[8]) to facilitate hierarchical assembly of uranyl metallacycles with higher complexity, and successfully prepare two different kinds of uranyl metallacycle-based complexes with intriguing hierarchical structures, a CB[7]-based four-member molecular necklace ([4]MN) and a CB[8]-involved ring-in-ring supramolecular polymer chain. The results obtained here prove the feasibility of supramolecular inclusion for regulating coordination assembly of uranyl metallacycles and related hierarchical structures. It is believed that this method can be used to achieve the construction of actinide coordination assemblies with higher structural complexity.

Metallacycles and metallacages, of which the synthesis always relies on coordination-driven self-assembly of metal centers with elegantly tailored angular ligands [1–4], are typical supramolecular coordination complexes (SCCs) [5–10] featuring discrete closed structures with well-defined shapes and dimensions [6,7,11]. These finite supramolecular architectures can be used in different fields such as biomedical sensor [12], electrochemistry [13] or "smart" soft materials [14–16]. Up to now, metal nodes used in metallacycles or metallacages with different degrees of structural complexity are mainly transition metals [2,7,9,10] and lanthanides [17–21]. Recently, actinide ions are introduced as an emerging class of metal nodes for the construction of supramolecular metallacycles. For example, uranium, a most-studied actinide element that exists in nature as a stable uranyl ion with two axial oxygens, are employed in many discrete architectures with closed structures such as metal-coordinated macrocycles [22–24], and nanocages [25–27]. It should be mentioned that, although the rich coordination chemistry of actinide nodes (*e.g.,* uranyl sphere could be tetragonal bipyramid, pentagonal bipyramid or hexagonal bipyramid) has facilitated the preparation of various discrete coordination assemblies, most of the current work is still mainly touch upon coordination-based primary assembly, while further multi-level assembly of these building blocks toward hierarchical supramolecular structures are still rarely investigated.

Multi-level assembly of complex hierarchical structures from well-defined supramolecular units has attracted the interest of supramolecular chemists and material specialists [16,17,28–31]. Many elegant examples of complex hierarchical structures are observed in biological systems, such as molecular knots, links, and entanglements found in the helix of DNA, the folding of RNA, and the multi-level assembly of proteins in natural organisms [32]. These exquisite artificial assemblies can help us better understand the mechanisms of self-assembly in nature, and also offer valuable hints to make complex biomimetic materials with desirable structures and functionality. The hierarchical assembly is always facilitated by non-covalent interactions [33–35], including electrostatic interactions, hydrophobic interactions, hydrogen bonds and π-π interactions *etc.,* which play important role in linking different subunits together. Compared with covalent interactions, non-covalent interactions fall into the range of weak intermolecular interactions that is intrinsically flexible and dynamic. With the aid of these weak interactions, those independent but interacting discrete supramolecular motifs can aggerate together and assemble to form final hierarchical assemblies.

* Corresponding authors.
E-mail addresses: meil@ihep.ac.cn (L. Mei), shiwq@ihep.ac.cn (W. Shi).

https://doi.org/10.1016/j.cclet.2022.03.092
1001-8417/

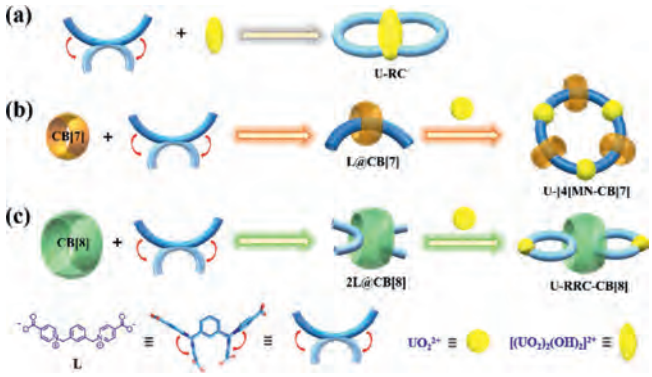

Scheme. 1. Self-assembly processes between uranyl node and the flexible L linker without or with macrocyclic cucurbituril hosts: (a) dinuclear uranyl-sealed metallacycle U-RC formed from coordination assembly of L and dimeric uranyl node; (b) CB[7]-enabled formation of uranyl-based [4]MN, U-[4]MN-CB[7], through a L@CB[7] pseudorotaxane linker; (c) CB[8]-enabled formation of ring-in-ring supramolecular polymer chain (U-RRC–CB[8]) through a 2L@CB[8] pseudorotaxane linker.

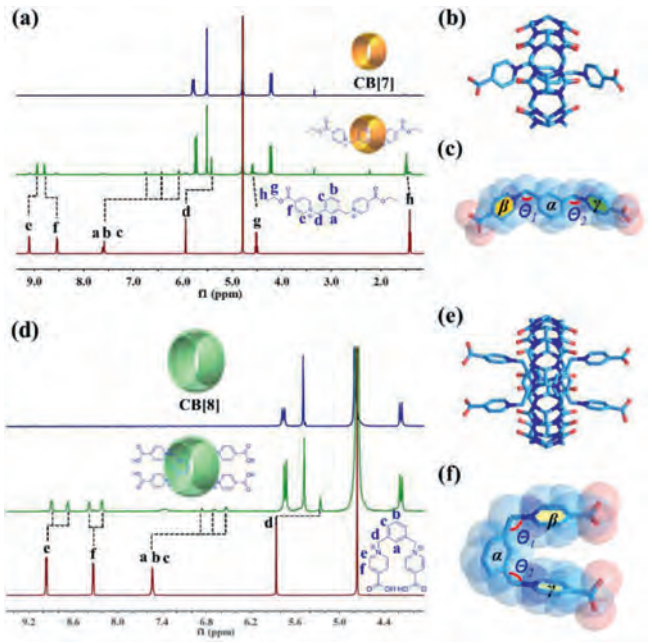

Fig. 1. Supramolecular inclusion between L and two cucurbituril macrocycles, CB[7] and CB[8], and crystal structures of the corresponding pseudorotaxane, L@CB7 and 2L@CB8. (a) ^{1}H NMR spectra (500 MHz, D_2O, 298 K) of a mixture of CB[7] and an equimolar amount of $L_{OET}Br_2$ with that of CB[7] and $L_{OET}Br_2$ as a comparison; (b) Crystal structure of L@CB[7]; (c) The structure of individual L in L@CB[7], showing the characteristic angles; (d) ^{1}H NMR spectra (500 MHz, D_2O, 298 K) of 2L@CB[8] with that of CB[8] and $[H_2L]Br_2$ as a comparison; (e) Crystal structure of 2L@CB[8]; (f) The structure of individual L in 2L@CB[8], showing the characteristic angles. Solvent molecules have been omitted for the sake of clarity. C sky blue, O red, N dark blue.

In pursuit of coordination-driven self-assembly of actinide metallacycles, we have used a flexible 'U'-shape *o*-xylene-derived dicarboxylate ligand (L: 1,1′-(1,3-phenylenebis(methylene)) bis(pyridin-1-ium-4-carboxylate)) to construct a binuclear uranyl-sealed metallacycle, U-RC (Scheme 1a) [23]. Herein, we further explore the multi-level assembly of this two-component metal-ligand (uranyl-L) system. A novel supramolecular inclusion-based method through introducing two different kinds of macrocyclic hosts, cucurbit[7]uril (CB[7]) and cucurbit[8]uril (CB[8]) are proposed to facilitate possible interactions of uranyl-L system with a third component toward induced formation of hierarchical assembly structures with higher complexity. The results reveal that, both supramolecular inclusions by macrocyclic CB[7] and CB[8] of L with a flexible skeleton exert a significant effect on its molecular conformation, as well as its coordination assembly with uranyl. It should be noted that, due to the difference in supramolecular inclusion behavior between the guest L and CB[7]/CB[8] macrocycles, two completely different assembly pathways can be observed (Schemes 1b and c). As a consequence, the final topologic structures of the resulting uranyl metallacycles and their secondary assembly with macrocyclic motifs are totally different, where the involvement of CB[7] leads to the formation of a four-member [4]MN, U-[4]MN–CB[7], through a L@CB[7] pseudorotaxane linker (Scheme 1b), while CB[8] facilitates the assembly of a ring-in-ring supramolecular polymer chain (U-RRC-CB[8]) through a 2L@CB[8] pseudorotaxane linker, among which a pair of adjacent figure-8 monomeric uranyl-based metallacycles are welded by CB[8] (Scheme 1c).

The supramolecular inclusion between the starting reactant $L_{OET}Br_2$ [23], the ethyl ester of L linker, and two cucurbituril macrocycles were first investigated. ^{1}H NMR analysis (Fig. 1a and Fig. S5 in Supporting information) shows that chemical environments of the guest hydrogen atoms undergo changes upon mixing with CB[7]. Besides a small amount of signals assigned to residual non-encapsulated $L_{OET}Br_2$, a new set of CB[7]-encapsulated species can be observed, indicating that the transformation between the threading and unthreading processes for $L_{OET}Br_2$ and CB[7] undergoes a slow kinetic on the NMR time scale. Detailed assignation of these NMR signals shows that the chemical shifts of four hydrogen atoms (H_a, H_b, H_c and H_d) of the 1,3-xylenyl group at the center of $L_{OET}Br_2$ move upfield, while both H_g and H_h of the ethyl group have minor downfield shifts, indicating that CB[7] is likely to bind at the 1,3-xylene site in the form of a pseudorotaxane. The pseudorotaxane structure between $L_{OET}Br_2$ and CB[7] can be further confirmed by single-crystal structure analysis given below, though NOE signals between $L_{OET}Br_2$ and CB[7] can hardly be observed due to the long distance between the hydrogen atoms on the benzene ring of $L_{OET}Br_2$ in the middle of the guest are far away from the hydrogen atoms on CB[7] (Fig. S6 in Supporting information, the precise molecular structure is extracted from the crystal structure discussed below). Furthermore, Job-plot (Fig. S7 in Supporting information) reveal that the stoichiometric ratio in a pseudorotaxane of $L_{OET}Br_2$ and CB[7] is 1:1, which is consistent with the results of mass spectrometry analysis (Fig. S8 in Supporting information). The corresponding pseudorotaxane crystals are prepared hydrothermally, and subject to X-ray crystallographic analysis (Fig. 1b, Fig. S9 and Table S1 in Supporting information). The result reveals that, as expected, each L guest is encapsulated by one CB[7] at the central site of 1,3-xylenyl to form a L@CB[7]-type pseudototaxane. A similar inclusion complex has been reported in a CB[7]-based pseudorotaxane with a 1,4-xylenyl analogue as the guest molecule [36], though the 1,3-substitution isomerization enables L to stretch out in the shape of letter 'M' with an opening angle (the dihedral angle between plane β and plane γ) of 296.359° (Fig. 1c).

The binding affinity of L to CB[8] was also investigated using ^{1}H NMR (Fig. 1d). Hydrogen atoms of 1,3-xylenyl group (H_a, H_b, H_c and H_d) show upfield shifts similar to that in L@CB[7] pseudorotaxane, while both the signals of H_e and H_f are split into two independent peaks. This splitting phenomenon suggests that the space around each terminal pyridinium may be interfered by other groups, resulting in a change in its chemical environment, which finally causes all the hydrogen atoms on the pyridinium ring to no longer be chemically equivalent. A plausible explanation is that the inclusion between L and CB[8] with a larger cavity takes a different pattern than the case involving CB[7]. X-ray crystallographic anal-

ysis of crystals based on both components of CB[8] and L shows that, the L guest adopts a 'U'-shaped folded configuration with an opening angle (the dihedral angle between plane β and plane γ) of 15.562° in CB[8] macrocycle with a larger cavity than CB[7] (Figs. 1e and f, Fig. S10 in Supporting information), where both terminal pyridinium groups are close to each other and show a certain degree of mutual interactions. This special conformation of L is consistent with the above ^{1}H NMR results. Moreover, the large cavity of CB[8] macrocycle can accommodate two U-shaped guests at the same time, which are partially pushed out to the outer space of the overcrowded CB[8] cavity in this 2L@CB[8] pseudorotaxane (Fig. 1e). The relatively less endocytosis of L guest into the cavity of CB[8] makes intermolecular interactions between them more or less weakened, which can be confirmed from the reduced magnitude of chemical shift change (H_a, H_b and H_c) compared to that of L@CB[7] and mass spectrometry (only low-intensity partially decomposed fragments of 2L@CB[8] can be observed in Fig. S11 in Supporting information). Another interesting phenomenon is the deformation of CB[8] (7.9 Å and 10.4 Å, Fig. S12 in Supporting information) compared to CB[7], which might be originated from the unique inclusion behavior of CB[8].

The above results on supramolecular inclusion of L with CB[7] and CB[8] demonstrate that, due to distinct cavity sizes of CB[7] and CB[8], their inclusion behaviors with the flexible guest L are different, thus resulting in significant difference in assembly pattern and molecular conformation of as-formed pseudorotaxanes, L@CB[7] and 2L@CB[8]. It can be expected that this interesting macrocycle-based regulation method will greatly affect the coordination mode and supramolecular assembly of the pseudorotaxane linker. Therefore, the coordination assembly of L@CB[7] or 2L@CB[8] with uranyl is further explored.

Hydrothermal reaction of L@CB[7] and uranyl, or alternately, a direct one-pot reaction of uranyl, $L_{OET}Br_2$ and CB[7], produces yellow block crystals of U-[4]MN-CB[7], which are subject to single-crystal determination. Crystallographic analysis (Tables S2-S4 in Supporting information) shows that, in the asymmetric unit of U-[4]MN-CB[7], there are three L@CB[7] linkers that are connected in a monodentate mode by three monomeric uranyl centers to form a cationic molecular loop with three threaded CB[7] macrocycles, thus being namely as [4]-MN (Figs. 2a-d and Fig. S13 in Supporting information). Interestingly, since the introduction of CB[7], the topological structure of U-[4]MN-CB[7] is totally different from that of U-RC without CB[7] involved. It is no doubt that the increase of opening angle of flexible L linker (the dihedral angle between plane β and plane γ is 289.763° in U-[4]MN-CB[7], Fig. 2c) driven by CB[7] is crucial to promote the formation of this large closed metallacycle (U-U distances: 18.718, 19.165 and 19.056 Å). In spite of a minor deviation of experimental PXRD pattern from the simulated one relevant to partial solvent loss in the loosely-packing lattice of uranyl metallacycle of U-MN-CB[7] (Fig. S13 in Supporting information), the phase purity of U-[4]MN-CB[7] can still be verified (Fig. S14 in Supporting information). Characterization on its physico-chemical properties is also conducted (Figs. S15 and S16 in Supporting information).

The coordination assembly of uranyl with a mixture of $L_{OET}Br_2$ and CB[8] or directly with 2L@CB[8] affords yellow flake cluster crystals of U-RRC-CB[8]. Crystallographic analysis reveals that the CB[8]-involving pseudorotaxane motifs retains the same molecular conformation as that in 2L@CB[8], *i.e.,* with a pair of 'U'-shaped L linker trapped in the cavity of CB[8]. An array of such 2L@CB[8] are further connected by monomeric uranyl nodes to form a ring-in-ring cationic supramolecular polymer chain (Figs. 2e-h and Fig. S17 in Supporting information), among which each 'U'-shaped L linker bites the same uranyl center through two terminal monodentate carboxylate group. Characterization of physico-chemical properties were also conducted to prove its identity (Figs. S18-S20 in Supporting information).

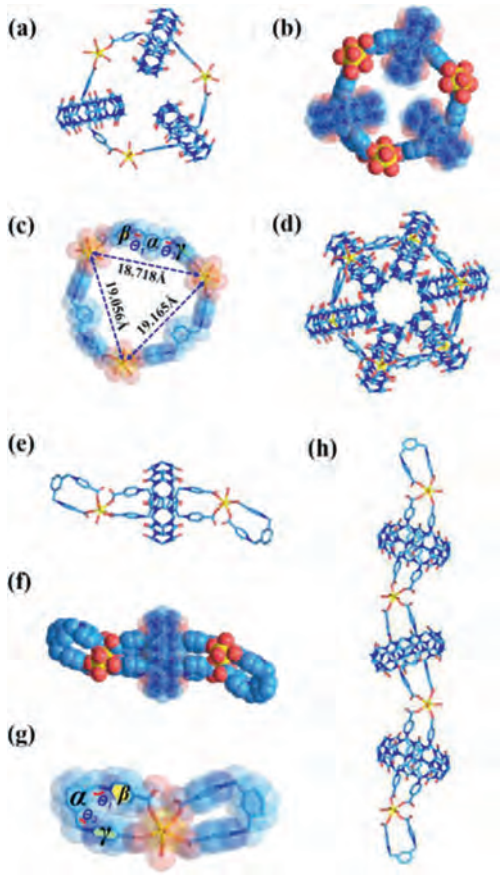

Fig. 2. Crystal structures of U-[4]MN-CB[7] and U-RRC-CB[8]. Capped-stick (a) and space-filling (b) representation of U-[4]MN-CB[7]. (c) The structure of individual ring in U-[4]MN–CB[7], showing the characteristic angles. (d) Stacked structure of U-[4]MN-CB[7]. Capped-stick (e) and space-filling (f) representation of U-RCC-CB[8]. (g) The structure of individual ring in U-RRC-CB[8], showing the characteristic angles. (h) Stacked structure of U-RRC-CB[8]. Solvent molecules have been omitted for the sake of clarity. U yellow, C sky blue, O red, N dark blue (the phenyl group is defined as plane α, while the pyridinium rings are plane β and γ, see Tables S5-S6 in Supporting information for details).

The coordination pattern of L linker with uranyl in U-RRC-CB[8] is very similar to that observed in U-RC, and the only difference is the nuclearity of uranyl node, which evolutes from dimeric uranyl in U-RC to monomeric U-RRC-CB[8] Similar to 2L@CB8, a exacerbated folding of 'U'-shaped L linker enforced by the surrounding CB[8] macrocycle through supramolecular inclusion plays an important role, where the opening angle in U-RRC-CB[8] is reduced to −18.621° (the minus signal means the direction of opening angle is reversed) accompanied with two terminal carboxyl groups getting closer.

A further detailed comparison of L linkers in L@CB[7], U-[4]MN-CB[7], 2L@CB[8], U-RRC-CB[8] and U-RC are conducted to unveil the effect of supramolecular inclusion on hierarchical assembly of uranyl metallacycles and the minor structural changes of L linkers after uranyl coordination (Table S5 and S6 in Supporting information). First, it can be seen that, the introduction of macrocyclic host for supramolecular inclusion of the L linker, compared to U-RC, greatly alters the coordination assembly process of uranyl metallacycles. More importantly, the nature of macrocycles, such as CB[7] and CB[8] used here with different dimensions and supramolecular inclusion behaviors, also has a significant impact and would lead to different outcomes of metallacycle-based hierarchical assemblies. As demonstrated above, CB[7] with a smaller cavity is threaded by one guest molecule, while CB[8] with a larger cav-

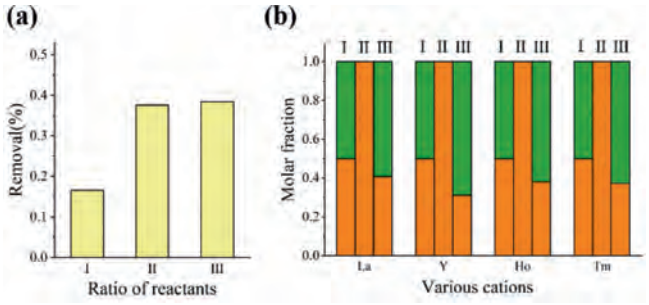

Fig. 3. (a) The removal rate of U with different ratios of ligand and uranyl ion (I represent $L_{OET}Br_2$:CB[7]:U = 1:1:1, II represent $L_{OET}Br_2$:CB[7]:U = 2:2:1 and III represent $L_{OET}Br_2$:CB[7]:U = 3:3:1). (b) separation results of U/M crystallization experiment when $L_{OET}Br_2$:CB[7]:U = 3:3:1 (I, II and III columns represent the molar distribution of U/M in the starting material, crystals and wash solutions, respectively).

ity can contains two folded guest molecules at the same time. Along this line, the degree of macrocycle-induced conformational restriction of each guest molecule varies with the type of macrocycles. As a result, the bipyridinium guest in the pseudorotaxane formed by supramolecular inclusion of CB[7] has a large opening angle, and it can assemble with uranyl ion to obtain a [4]MN; on the other hand, the opening angle of the guest linker after encapsulated by CB[8] is further restrained, and it can only accommodates a mononuclear uranyl ion to obtain a uranyl metallacycle. Furthermore, metal coordination will also exert impact on ligand conformation. For example, after coordination with uranyl, the opening angle and distance between two end carboxyl of the L linker in 2L@CB[8] are also significantly reduced (before coordination, 15.562° and 6.076 Å; after coordination, −18.621° and 4.296 Å, Table S6), which is related to the structural adjustment of flexible L linker so as to meet the requirement of metal coordination.

Finally, we explore the crystallization separation of uranyl ions based on the fact that U-[4]MN-CB[7] tends to crystallize out from the solution. The primary separation experiment shows that the removal rate of uranyl increases with the ratio of ligand-to-uranyl and reaches to *ca.* 40% when the ratio is over 2:2:1 (Fig. 3a). The removal rate of U here should be restrained by relatively high equilibrium concentrations of U and L@CB7, which might be originated from the modest binding affinity between uranyl and the carboxyl group of L@CB7. The selective separation of uranyl is further evaluated. Control experiments reveal that L@CB[7] does not interact with other metal centers when using other metal sources such as typical lanthanide ions. Therefore, this coordination assembly method is expected to be used for the selective crystallization separation of uranyl ions from lanthanide ions. A competitive experiment shows that the crystallization of high-purity U-[4]MN-CB[7] crystals can still proceed smoothly even in the presence of other lanthanide ions from La^{3+} to Yb^{3+} (Fig. 3b, Figs. S21 and S22 in Supporting information).

In summary, we introduce two different kinds of macrocyclic hosts to facilitate supramolecular inclusion of a flexible organic linker and thus regulate the hierarchical self-assembly of uranyl metallacycles. Ultimately, the encapsulation of CB[7] makes the guest linker to stretch out with a large opening angle and leads to the formation of a [4]MN, while CB[8] restrains the guest linker to be 'U'-shaped with a smaller opening angle, and promotes the assembly of a ring-in-ring supramolecular polymer chain. This work provides a feasible method for the construction of actinide metallacycles with higher structural complexity, and enriches the library of actinide coordination assemblies. More work on the applications of coordination-driven assemblies in crystallization separation of actinide will be conducted in future.

Declaration of competing interest

The authors declare that they have no known competing financial interests or personal relationships that could have appeared to influence the work reported in this paper.

Acknowledgments

We thank the support from the National Science Fund for Distinguished Young Scholars (No. 21925603) and the National Natural Science Foundation of China (Nos. 22122609, 22076186 and 22176191).

Supplementary materials

Supplementary material associated with this article can be found, in the online version, at doi:10.1016/j.cclet.2022.03.092.

References

[1] B. Moulton, M.J. Zaworotko, Chem. Rev. 101 (2001) 1629–1658.
[2] H. Li, Z.J. Yao, D. Liu, G.X. Jin, Coord. Chem. Rev. 293 (2015) 139–157.
[3] D.W. Zhang, T.K. Ronson, J.R. Nitschke, Acc. Chem. Res. 51 (2018) 2423–2436.
[4] L. Chen, Q.H. Chen, M.Y. Wu, F.L. Jiang, M.C. Hong, Acc. Chem. Res. 48 (2015) 201–210.
[5] T.R. Cook, Y.R. Zheng, P.J. Stang, Chem. Rev. 113 (2013) 734–777.
[6] R. Chakrabarty, P.S. Mukherjee, P.J. Stang, Chem. Rev. 111 (2011) 6810–6918.
[7] T.R. Cook, P.J. Stang, Chem. Rev. 115 (2015) 7001–7045.
[8] W. Wang, Y.X. Wang, H.B. Yang, Chem. Soc. Rev. 45. (2016) 2656–2693.
[9] W.X. Gao, H.J. Feng, B.B. Guo, Y. Lu, G.X. Jin, Chem. Rev. 120 (2020) 6288–6325.
[10] S. Datta, M.L. Saha, P.J. Stang, Acc. Chem. Res. 51 (2018) 2047–2063.
[11] R.S. Forgan, J.P. Sauvage, J.F. Stoddart, Chem. Rev. 111 (2011) 5434–5464.
[12] T.R. Cook, V. Vajpayee, M.H. Lee, P.J. Stang, K.W. Chi, Acc. Chem. Res. 46 (2013) 2464–2474.
[13] L. Xu, Y.X. Wang, L.J. Chen, H.B. Yang, Chem. Soc. Rev. 44 (2015) 2148–2167.
[14] Y.X. Hu, X.Y. Zhang, L. Xu, H.B. Yang, Isr. J. Chem. 59 (2019) 184–196.
[15] B.H. Northrop, H.B. Yang, P.J. Stang, Chem. Commun. 45 (2008) 5896–5908.
[16] L.J. Chen, H.B. Yang, Acc. Chem. Res. 51 (2018) 2699–2710.
[17] X.Q. Guo, L.P. Zhou, S.J. Hu, et al., J. Am. Chem. Soc. 143 (2021) 6202–6210.
[18] Z. Wang, L.Z. He, B.Q. Liu, et al., J. Am. Chem. Soc. 142 (2020) 16409–16419.
[19] C.L. Liu, R.L. Zhang, C.S. Lin, et al., J. Am. Chem. Soc. 139 (2017) 12474–12479.
[20] X.Z. Li, L.P. Zhou, L.L. Yang, et al., J. Am. Chem. Soc. 139 (2017) 8237–8244.
[21] X.Z. Li, L.P. Zhou, L.L. Yan, et al., Nat. Commun. 9 (2018) 547.
[22] P. Thuery, C. Villiers, J. Jaud, M. Ephritikhine, B. Masci, J. Am. Chem. Soc. 126 (2004) 6838–6839.
[23] S. Wu, L. Mei, K.Q. Hu, et al., J. Inorg. Mater. 118 (2019) 243–249.
[24] J. Lee, J.T. Brewster, B. Song, et al., Chem. Commun. 54 (2018) 9422–9425.
[25] S. Pasquale, S. Sattin, E.C. Escudero-Adan, M. Martinez-Belmonte, J. de Mendoza, Nat. Commun. 3 (2012) 785.
[26] L. Mei, P. Ren, Q.Y. Wu, et al., J. Am. Chem. Soc. 142 (2020) 16538–16545.
[27] L.W. Cheng, C.Y. Liang, W. Liu, et al., J. Am. Chem. Soc. 142 (2020) 16218–16222.
[28] L. Shao, X.Q. Hu, K. Sikligar, G.A. Baker, J.L. Atwood, Acc. Chem. Res. 54 (2021) 3191–3203.
[29] D. Fujita, Y. Ueda, S. Sato, N. Mizuno, T. Kumasaka, M. Fujita, Nature 540 (2016) 563–566.
[30] H.B. Qiu, Z.M. Hudson, M.A. Winnik, I. Manners, Science 347 (2015) 1329–1332.
[31] P.J. Santos, P.A. Gabrys, L.Z. Zornberg, M.S. Lee, R.J. Macfarlane, Nature 591 (2021) 586–591.
[32] D.D. Boehr, R. Nussinov, P.E. Wright, Nat. Chem. Biol. 5 (2009) 789–796.
[33] J.M. Lehn, Chem. Soc. Rev. 46 (2017) 2378–2379.
[34] D.Y. Xia, P. Wang, X.F. Ji, et al., Chem. Rev. 120 (2020) 6070–6123.
[35] J.M. Lehn, Abstr. Pap. Am. Chem. S. 199 (1990) 399.
[36] L. Mei, Z.N. Xie, K.Q. Hu, et al., Chem. Eur. J. 23 (2017) 13995–14003.